Metal–Organic Frameworks

International Edition: DOI: 10.1002/anie.201711725
German Edition: DOI: 10.1002/ange.201711725

Integration of Plasmonic Effects and Schottky Junctions into Metal–Organic Framework Composites: Steering Charge Flow for Enhanced Visible-Light Photocatalysis

*Juan-Ding Xiao, Lili Han, Jun Luo, Shu-Hong Yu, and Hai-Long Jiang**

Abstract: *A wide range of light absorption and rapid electron–hole separation are desired for efficient photocatalysis. Herein, on the basis of a semiconductor-like metal–organic framework (MOF), a Pt@MOF/Au catalyst with two types of metal–MOF interfaces integrates the surface plasmon resonance excitation of Au nanorods with a Pt-MOF Schottky junction, which not only extends the light absorption of the MOF from the UV to the visible region but also greatly accelerates charge transfer. The spatial separation of Pt and Au particles by the MOF further steers the formation of charge flow and expedites the charge migration. As a result, the Pt@MOF/Au presents an exceptionally high photocatalytic H_2 production rate by water splitting under visible light irradiation, far superior to Pt/MOF/Au, MOF/Au and other counterparts with similar Pt or Au contents, highlighting the important role of each component and the Pt location in the catalyst.*

Photocatalytic hydrogen (H_2) production by water splitting based on semiconductor catalysts is a highly promising solution to the demands of current energy and environmental issues.[1,2] The efficient photocatalytic H_2 production requires rapid separation of photogenerated electrons (e) from holes (h), allowing their delivery to specific sites for further proton reduction. Given that UV light accounts for only approximately 4% while visible light contributes to about 43% of solar energy, the extension of light absorption from UV to visible region will greatly improve light harvesting and also photocatalytic activity.[1] Therefore, the fabrication of a single photocatalyst that combines the broad range of light absorption and efficient e–h separation would be highly desired to boost the photocatalytic H_2 production.

Porous semiconductors aid substrate/product transport and the exposure of active sites,[2] which allows charge carriers to travel short distances to reach the internal surface of catalyst for subsequent redox reactions, largely suppresses e–h recombination. As semiconductor-like porous materials, metal–organic frameworks (MOFs),[3] assembled from metal ions/clusters and organic linkers, have demonstrated their potential in photocatalysis.[4–6] In addition to the common merits of porous semiconductors mentioned above, the crystalline nature of MOFs avoids structural defects, a type of e–h recombination centers. To suppress e–h recombination further, the introduction of electron sinks, such as metal nanoparticles (NPs), to n-type-semiconductor MOFs has been recognized as an effective strategy to improve charge separation,[6] whereby the migrated electrons are trapped by the metal across a junction because of the Schottky barrier, whereas holes freely diffuse to MOF surface (Scheme S1 in the Supporting Information). On the other hand, most MOFs behaving like semiconductors exhibit wide band gaps with a high conduction band (CB) and a low valence band (VB), which are crucial for the high redox ability of charge carriers but permit only UV light absorption, limiting solar energy utilization. The long-wavelength light absorption (low CB and/or high VB) and high redox ability are essentially irreconcilable contradiction for a single semiconductor photocatalyst. Alternatively, nanostructured metals (e.g., Au, Ag) possessing surface plasmon resonance (SPR) can be excited under visible light irradiation to generate and inject hot electrons into the lowest unoccupied molecular orbital (LUMO) or CB of n-type semiconductor-like MOFs.[7] The introduction of SPR into wide-band-gap photocatalysts, such as MOFs, would an effective strategy to extend their light absorption from the UV to the visible or even the near-IR region while maintaining their redox ability.[8]

With the above points in mind, we integrated the plasmonic effect and a Schottky junction into a MOF for the first time by forming two metal-MOF interfaces. One interface between the MOF and plasmonic metal nanocrystals is to inject plasmonic hot electrons into the LUMO of the MOF, allowing long-wavelength light absorption. The other nonplasmonic metal-MOF interface is to establish a Schottky barrier as the charge "pump", which steers the unidirectional electron flow to be trapped by the metal (electron acceptor) across the interface, thus greatly promoting the e–h separation and photocatalytic efficiency. Therefore, this design offers a platform to utilize semiconductor-like MOFs or other porous materials, featuring a high redox ability but also wide band gaps, for efficient photocatalysis by harvesting as wide a range of sunlight wavelengths as possible.

Herein, a representative MOF behaving as wide-band-gap semiconductor, MIL-125,[9] was investigated as a UV-respon-

[*] J.-D. Xiao, Prof. Dr. S. H. Yu, Prof. Dr. H.-L. Jiang
Hefei National Laboratory for Physical Sciences at the Microscale, CAS Key Laboratory of Soft Matter Chemistry, Collaborative Innovation Center of Suzhou Nano Science and Technology, Department of Chemistry, University of Science and Technology of China
Hefei, Anhui 230026 (P. R. China)
E-mail: jianglab@ustc.edu.cn
Homepage: http://staff.ustc.edu.cn/~jianglab/
Dr. L. Han, Prof. Dr. J. Luo
Center for Electron Microscopy, Institute for New Energy Materials and Low-Carbon Technologies, School of Materials, Tianjin University of Technology
Tianjin 300384 (P. R. China)
Supporting information and the ORCID identification number(s) for the author(s) of this article can be found under: https://doi.org/10.1002/anie.201711725.

sive photocatalyst. To build Schottky junction, Pt NPs as electron acceptors were dispersed into or supported on MIL-125 to afford Pt@MIL-125 and Pt/MIL-125, respectively. Subsequently, the plasmonic Au nanorods (NRs), possessing SPR excitation in the visible region, were assembled onto Pt@MIL-125, Pt/MIL-125, and pure MIL-125 to, respectively, give Pt@MIL-125/Au, Pt/MIL-125/Au, and MIL-125/Au (Scheme 1). The spatial position of Pt NPs relative to MOF

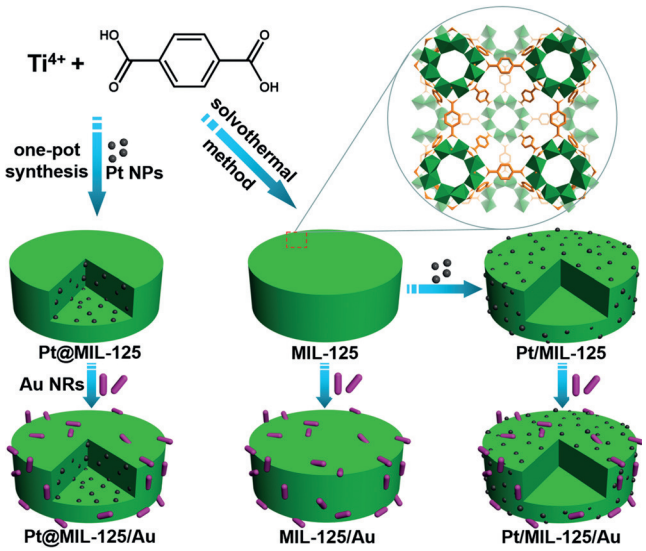

Scheme 1. Schematic illustration showing the synthesis of Pt@MIL-125/Au and the corresponding Pt/MIL-125/Au and MIL-125/Au analogues.

greatly influences the photocatalytic activity and the e–h recombination can be more effectively suppressed in Pt@MIL-125 than Pt/MIL-125. As a result, Pt@MIL-125/Au exhibits much higher visible-light photocatalytic H_2 production activity than all others. As far as we know, this is the first report on synergetic utilization of the plasmonic effect and a Schottky junction to extend the visible light absorption of MOFs and promote e–h separation for efficient photocatalysis.

The MIL-125 with sizes of approximately 500 nm and Pt NPs of about 3 nm (Figure S1) were pre-synthesized based on the documented methods.[6e,9c] The Pt location to MIL-125 can be controlled by adjusting the timing of the introduction of the Pt NPs during the synthetic process (Scheme 1; Supporting Information Section 2).[6e,i] Simply, Pt@MIL-125 was obtained by pre-introducing Pt NPs into the reactants for preparing MIL-125, whereas Pt/MIL-125 was formed by adding Pt NPs solution to MIL-125 for subsequent assembly. The Pt@MIL-125 with 0.49 wt% Pt loading was optimized to display excellent Pt dispersion inside the MOF particles (Figure 1a). Pt/MIL-125 with similar Pt content (0.47 wt%) features well-dispersed Pt NPs on the entire MOF external surface (Figure 1b). The Pt NPs remain approximately 3 nm regardless of whether they are dispersed into or onto MOF, as shown by transmission electron microscopy (TEM) observations (Figure S2). For Pt@MIL-125, the internal Pt location was unambiguously demonstrated by the high-angle annular

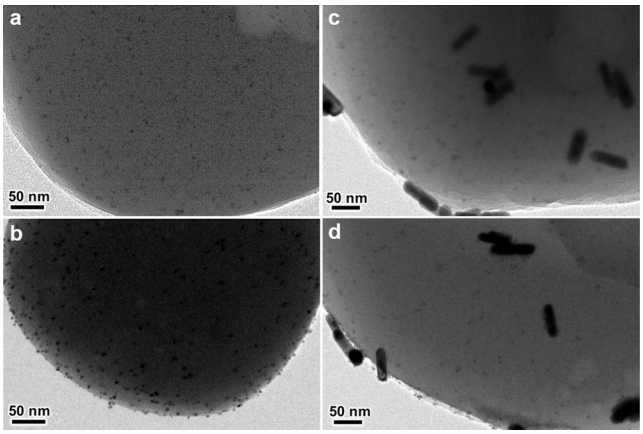

Figure 1. Typical TEM images of a) Pt@MIL-125, b) Pt/MIL-125, c) Pt@MIL-125/Au, and d) Pt/MIL-125/Au.

dark-field scanning TEM (HAADF-STEM) tomography and 3D reconstruction results (Figure S3 and the Supporting Videos).

The Au NRs with sizes of $(52 \pm 3\ \text{nm}) \times (14 \pm 3\ \text{nm})$ show SPR peaks centered at around 700 nm (Figure S4 and S5).[10] They were then assembled onto Pt@MIL-125 to afford Pt@MIL-125/Au with 2.81 wt% Au loading. Two reference catalysts of MIL-125/Au and Pt/MIL-125/Au with similar Au contents of 3.01 wt% and 2.74 wt%, respectively, were also obtained. Zeta potentials of MIL-125 and Au NRs in aqueous solution were measured to be -11.1 and $+32.9$ mV, respectively, indicating their close contact via electrostatic interaction and the presence of high-quality Au-MOF interfaces (Figure 1c,d; Figure S6). The crystallinity of MIL-125 almost remains after loading Pt NPs or/and Au NRs based on powder X-ray diffraction (PXRD) profiles (Figure S7). The diffraction peaks of Pt NPs are unobservable due to their small sizes and low contents. The identifiable diffraction peaks at around 38° are assignable to the (111) facet of Au NRs.[8c,d] N_2 sorption isotherms demonstrate their similar porous characters (Figure S8). Slight decrease of BET surface areas for the Au-decorated products should be ascribed to the mass contribution of Au NRs, whereas the influence of Pt NPs is negligible due to their very low contents. These important features and fixed Pt and Au contents make it reasonable to compare the activity of Pt@MIL-125/Au with Pt@MIL-125, MIL-125/Au, Pt/MIL-125/Au and other related photocatalysts.

The optical responses of Pt@MIL-125/Au and reference samples were examined by UV/Vis spectra (Figure 2a). The bare MIL-125 and Pt/MIL-125 have no absorption in the visible region, except for the high scattering of Pt@MIL-125 caused by Pt NPs.[6e,11] After assembling Au NRs with these samples, a new absorption band at approximately 700 nm is assignable to SPR excitation of Au NRs (Figure 2a, inset), suggesting that all catalysts involving Au NRs and MIL-125 possess comparable light absorption. Photoluminescence (PL) emission spectroscopy offers important hints for photo-induced charge transfer and recombination. The PL intensity is slightly weakened after supporting Pt NPs onto MIL-125/Au while it is almost quenched upon incorporating

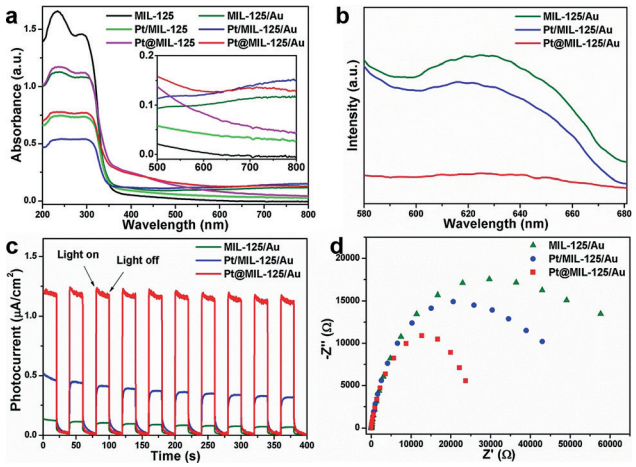

Figure 2. a) UV/Vis diffuse reflectance spectra for different catalysts (inset: selected range of 500–800 nm). b) PL emission spectra (λ_{ex} = 455 nm), c) photocurrent responses, and d) EIS Nyquist plots for MIL-125/Au, Pt/MIL-125/Au, and Pt@MIL-125/Au.

Pt NPs into MIL-125/Au (Figure 2b), suggesting the manipulation of Pt-MOF Schottky junction is able to prevent the radiative e-h recombination. Moreover, thanks to the more effective spatial separation of Pt and Au, Pt@MIL-125/Au presents much better charge separation efficiency than Pt/MIL-125/Au and other samples, as proved by photocurrent results (Figure 2c; Figure S9a). In addition, these are also supported by electrochemical impedance spectroscopy (EIS) (Figure 2d; Figure S9b), in which Pt@MIL-125/Au exhibits the smallest radius, implying the lowest charge-transfer resistance. The distinctly different optical and electrochemical properties among the samples mentioned above infer their possible difference in photocatalytic activity and the best performance of Pt@MIL-125/Au is expected.

We then set out to investigate the photocatalytic H_2 production by water splitting under visible-light irradiation. As displayed in Figure 3a, the reference catalysts MIL-125, Pt/MIL-125, and Pt@MIL-125 gave negligible activities. When Au NRs were supported on MIL-125, trace H_2 with poor photocatalytic activity of 10.2 μmol g^{-1} h was detected. Note that MIL-125 cannot be excited by visible light, and the above activity exactly reflects the Au plasmonic effect. Despite the poor activity of MIL-125/Au, its color changed from gray to blue under light irradiation,[5a,6g] indicating that Ti^{4+} was reduced to Ti^{3+} in MIL-125 by injected electrons from Au SPR and the situation can be hold for a certain time. Upon introducing Pt NPs to the reaction system, this color change quickly disappeared (Figure S10). The phenomena unambiguously verify that the formation of Pt-MOF Schottky junction steers the rapid electron migration from Ti^{3+} to Pt, promoting the subsequent proton reduction. As a result, compared to MIL-125/Au, both Pt/MIL-125/Au and Pt@MIL-125/Au exhibit exponential photocatalytic activity enhancement. Pt/MIL-125/Au shows H_2 production rate of 161.3 μmol g^{-1} h, ≈16 times higher than MIL-125/Au. Strikingly, with similar Pt and/or Au contents, Pt@MIL-125/Au possesses over two orders of magnitude activity enhancement (1743.0 μmol g^{-1} h, ca. 170 times) in reference to MIL-125/Au and over 10 times of Pt/MIL-125/Au. The turnover number of Pt@MIL-125/Au at 100 h is 1677 based on Pt and H_2 production continues after 100 h (Figure S11). Moreover, the wavelength dependent H_2 production rate of Pt@MIL-125/Au coincides with the plasmon band of Au NRs (Figure S12), revealing the photoreaction proceeds based on light absorption originated from Au SPR effect.

To reveal the optimal Au content, Pt@MIL-125/Au with different Au loadings (1.15, 2.08, 2.81, and 4.02 wt%) have been investigated under similar conditions (Figure S13). Results show that Pt@MIL-125/Au with 2.81 wt% Au loading, which is the default value hereafter otherwise stated, exhibits the highest activity (Figure S14). Significantly, the H_2 production rates over Pt@MIL-125/Au with different Au contents are much higher than that of Pt/MIL-125/Au, which reveals the structure advantage of Pt@MIL-125/Au and highlights the strong correlation between Pt location and activity. The spatial separation of Pt and Au by MIL-125 is assumed to be crucial to e–h separation, while the inevitable contact between Au and Pt in Pt/MIL-125/Au is detrimental. Moreover, the electron-transport distance is greatly shortened and electrons are quickly trapped by the well-incorporated Pt in Pt@MIL-125/Au,[6e] steering the generation of electron flow, which suppresses e–h recombination and thereby achieves much higher efficiency than Pt/MIL-125/Au. Further recycling experiments for Pt@MIL-125/Au demonstrate that no significant activity drop occurs during three catalytic runs (Figure 3b). PXRD profile and TEM image support the structural maintenance of Pt@MIL-125/Au after the reaction (Figure S15 and S16).

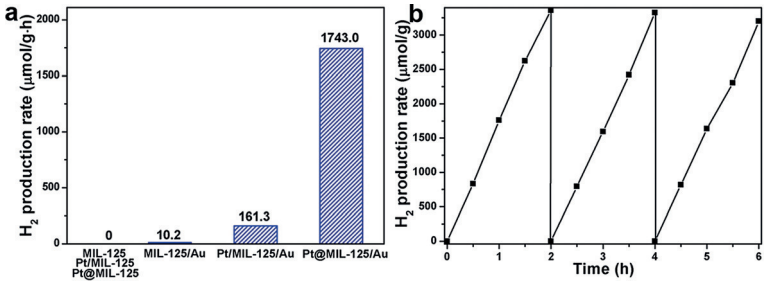

Figure 3. a) Photocatalytic H_2 production rates of different catalysts. b) Recycling performance of Pt@MIL-125/Au. The reaction with photocatalyst (5 mg) in MeCN/TEOA/H_2O (9:1:0.15 v/v, 20 mL) is irradiated by 380–800 nm light with a 300 W Xe lamp (LX-300F, Japan).

To decode how plasmonic effect of Au NRs and Pt-MOF Schottky junction synergistically boost the photocatalytic H_2 production, Mott–Schottky measurements in conjunction with electron spin resonance (ESR) tests have been conducted to elucidate the charge transfer process in Pt@MIL-125/Au. MIL-125 involves loop-shaped octamers by corner-sharing TiO_6 octahedra, which are photochromic related to the reduction of Ti^{4+} to Ti^{3+}.[12] To elucidate its semiconductor-like character, Mott-Schottky measurements at different frequencies have been carried out (Figure S17). The positive slope of the obtained C^{-2} value reveals the typical n-type semiconductor

behavior of MIL-125, indicating the hot electrons from Au NRs would migrate to the CB (LUMO) of MIL-125 rather than the delivery of hot holes to the VB (HOMO). The flat band position, which refers to LUMO in MIL-125,[5e] is determined from the intersection with value of −0.83 V versus Ag/AgCl (i.e., −0.63 V vs. normalized hydrogen electrode (NHE)). With the band gap of 3.72 eV estimated from Tauc plot (Figure S18), the HOMO of MIL-125 is then calculated (3.09 V vs. NHE). The more negative potential (−0.63 V) of MIL-125 than the reduction potential of H_2O to H_2 accounts for the feasibility of photocatalytic H_2 production.

Given MIL-125 is photo-responsive in UV region only, it does not present any ESR signal both in dark and under visible light irradiation (Figure 4a). Interestingly, MIL-125/Au in the dark shows a weak signal at *g* value of 2.002, which might be assignable to the oxygen defect in Ti-O clusters caused by unavoidable electron bombardment from Au.[6h,13] Upon visible-light irradiation for 300 s, ESR signal at 2.002 increases and a new signal at a *g* value of 1.947 appears, which can be attributed to Ti^{3+} intermediate generated in Ti-O clusters by more hot electrons from Au NRs.[6g,h] More importantly, Pt@MIL-125/Au gives the strongest Ti^{3+} signal compared with MIL-125/Au and Pt/MIL-125/Au (Figure 4b), explained by the greatly accelerated electron transfer process in Pt@MIL-125/Au. When light is switched off, the strong Ti^{3+} signal of Pt@MIL-125/Au disappears quickly (< 120 s), whereas that of MIL-125/Au is almost maintained even after 300 s, unambiguously manifesting the electron reservoir role of Pt NPs in Pt@MIL-125/Au (Figure S19). The results further suggest that, the deliberate spatial separation of Pt and Au in MIL-125, where Pt NPs are incorporated uniformly into the MOF and Au NRs are assembled on the MOF external surface—avoiding the light shielding effect, effectively guides the electron migration direction and promotes the rapid charge transfer. Such an elaborately fabricated catalyst steers electron flow for proton reduction and results in the highest photoactivity of Pt@MIL-125/Au observed above.

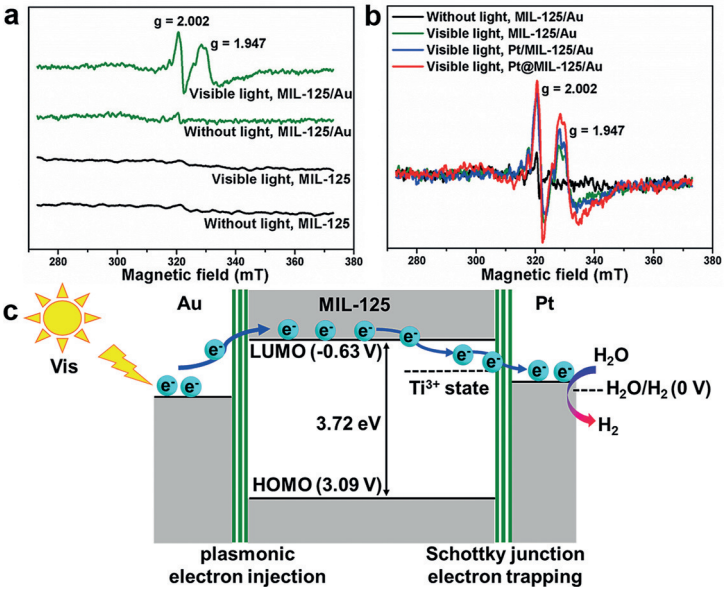

Figure 4. ESR spectra of a) MIL-125 and MIL-125/Au, and b) MIL-125/Au, Pt/MIL-125/Au, and Pt@MIL-125/Au at 140 K in the absence or presence of visible-light irradiation for 300 s. c) Schematic illustration showing the electron migration at the two metal–MOF interfaces based on the energy levels.

Based on the energy levels and the detected Ti^{3+} intermediate in the catalysts, the schematic depicting for the band alignments and charge flow at the two metal–MOF interfaces involved in the system is illustrated in Figure 4c. The charge flow steered in optimized Pt@MIL-125/Au catalyst system is mainly dominated by three aspects: 1) the plasmonic hot electrons from Au NRs triggered by visible light are injected to MOF, reducing Ti-O clusters to give Ti^{3+}; 2) the electrons are further delivered and trapped by Pt sites driven by Pt-MOF Schottky barrier; 3) the intrinsic spatial e–h separation and rapid electron consumption/reaction on Pt sites are due to the catalyst design. It is worth noting that the porous semiconductor-like MOF plays crucial roles to spatially separate Au and Pt to steer the charge flow for high catalytic efficiency and the composite catalyst is extendable by altering the three components. For instance, as a substitution of Au NRs, Au NPs have been used to fabricate Pt@MIL-125/Au(NPs), which also exhibits a high H_2 production rate due to comparable SPR effect of Au NPs (but shifted peak) under visible irradiation (Figure S20–22). Given that light absorption of Au NRs is readily extendable to near-infrared region by simply changing their aspect ratios, offering great opportunity toward more effective solar energy utilization in future endeavor. Therefore, though photocatalytic H_2 production activity of Pt@MIL-125/Au cannot achieve the best-level in previous reports (Table S1),[14] it is among the highest in MOF-based photocatalysts and the concept for this type of catalyst holds great promise for enhanced activity.

In summary, the uniform Pt NPs have been incorporated into or supported on a wide-band-gap MOF, MIL-125, to afford Pt@MIL-125 and Pt/MIL-125, respectively, which are further coated with Au NRs on the MOF surface to give Pt@MIL-125/Au and Pt/MIL-125/Au. The design of Pt@MIL-125/Au and Pt/MIL-125/Au achieves the synergetic utilization of long-wavelength light-driven plasmonic hot electron injection and Schottky junction electron trapping, which greatly improves solar energy utilization and e–h separation of MOF photocatalysts with wide band gaps. The resultant Pt@MIL-125/Au exhibits exponentially enhanced photocatalytic activity under visible light irradiation, compared with MIL-125/Au, Pt/MIL-125/Au, and other counterparts, demonstrating the composite catalyst is suitable for light harvesting and efficient charge separation. Though a MOF was employed, this work is based on the integration of the plasmonic effect and the Schottky junction, and takes a significant step forward to the utilization of a variety of porous wide-band-gap semiconductors for efficient photocatalysis by harvesting wide-wavelength sunlight.

Acknowledgements

We gratefully thank the reviewers for valuable suggestions, Dr. Jing Shi and Ms. Jinping Chen for support in STEM tomography observation. This work was supported by the NSFC (21725101, 21673213, 21371162, and 21521001), the National Research Fund for Fundamental Key Project (2014CB931803) and the Recruitment Program of Global Youth Experts.

Conflict of interest

The authors declare no conflict of interest.

Keywords: hydrogen production · metal–organic frameworks (MOFs) · photocatalysis · Schottky junction · surface plasmon resonance

How to cite: *Angew. Chem. Int. Ed.* **2018**, *57*, 1103–1107
Angew. Chem. **2018**, *130*, 1115–1119

[1] a) H. Tong, S. Ouyang, Y. Bi, N. Umezawa, M. Oshikiri, J. Ye, *Adv. Mater.* **2012**, *24*, 229; b) J. Ran, J. Zhang, J. Yu, M. Jaroniec, S. Z. Qiao, *Chem. Soc. Rev.* **2014**, *43*, 7787.

[2] a) W. Zhou, W. Li, J.-Q. Wang, Y. Qu, Y. Yang, Y. Xie, K. Zhang, L. Wang, H. Fu, D. Zhao, *J. Am. Chem. Soc.* **2014**, *136*, 9280; b) V. S. Vyas, F. Haase, L. Stegbauer, G. Savasci, F. Podjaski, C. Ochsenfeld, B. V. Lotsch, *Nat. Commun.* **2015**, *6*, 8508; c) Q. Lin, X. Bu, C. Mao, X. Zhao, K. Sasan, P. Feng, *J. Am. Chem. Soc.* **2015**, *137*, 6184.

[3] a) H.-C. Zhou, J. R. Long, O. M. Yaghi, *Chem. Rev.* **2012**, *112*, 673; b) H.-C. Zhou, S. Kitagawa, *Chem. Soc. Rev.* **2014**, *43*, 5415; c) Q.-L. Zhu, Q. Xu, *Chem. Soc. Rev.* **2014**, *43*, 5468; d) T. Devic, C. Serre, *Chem. Soc. Rev.* **2014**, *43*, 6097; e) T. Islamoglu, S. Goswami, Z. Li, A. J. Howarth, O. K. Farha, J. T. Hupp, *Acc. Chem. Res.* **2017**, *50*, 805; f) L. Zeng, X. Guo, C. He, C. Duan, *ACS Catal.* **2016**, *6*, 7935; g) B. Li, H.-M. Wen, Y. Cui, W. Zhou, G. Qian, B. Chen, *Adv. Mater.* **2016**, *28*, 8819; h) Q. Yang, Q. Xu, H.-L. Jiang, *Chem. Soc. Rev.* **2017**, *46*, 4774.

[4] a) T. Zhou, Y. Du, A. Borgna, J. Hong, Y. Wang, J. Han, W. Zhang, R. Xu, *Energy Environ. Sci.* **2013**, *6*, 3229; b) Y. Kataoka, K. Sato, Y. Miyazaki, K. Masuda, H. Tanaka, S. Naito, W. Mori, *Energy Environ. Sci.* **2009**, *2*, 397; c) A. Dhakshinamoorthy, A. M. Asiri, H. García, *Angew. Chem. Int. Ed.* **2016**, *55*, 5414; *Angew. Chem.* **2016**, *128*, 5504; d) S. Pullen, H. Fei, A. Orthaber, S. M. Cohen, S. Ott, *J. Am. Chem. Soc.* **2013**, *135*, 16997; e) S. Saha, G. Das, J. Thote, R. Banerjee, *J. Am. Chem. Soc.* **2014**, *136*, 14845; f) Y. An, Y. Liu, P. An, J. Dong, B. Xu, Y. Dai, X. Qin, X. Zhang, M.-H. Whangbo, B. Huang, *Angew. Chem. Int. Ed.* **2017**, *56*, 3036; *Angew. Chem.* **2017**, *129*, 3082; g) X. Dong, M. Zhang, R. Pei, Q. Wang, D. Wei, S.-Q. Zang, Y.-T. Fan, T. C. W. Mak, *Angew. Chem. Int. Ed.* **2016**, *55*, 2073; *Angew. Chem.* **2016**, *128*, 2113.

[5] a) Y. Fu, D. Sun, Y. Chen, R. Huang, Z. Ding, X. Fu, Z. Li, *Angew. Chem. Int. Ed.* **2012**, *51*, 3364; *Angew. Chem.* **2012**, *124*, 3420; b) K. G. M. Laurier, F. Vermoortele, R. Ameloot, D. E. De Vos, J. Hofkens, M. B. J. Roeffaers, *J. Am. Chem. Soc.* **2013**, *135*, 14488; c) S. Wang, W. Yao, J. Lin, Z. Ding, X. Wang, *Angew. Chem. Int. Ed.* **2014**, *53*, 1034; *Angew. Chem.* **2014**, *126*, 1052; d) H. Zhang, J. Wei, J. Dong, G. Liu, L. Shi, G. Zhao, J. Kong, X. Wang, X. Meng, J. Zhang, J. Ye, *Angew. Chem. Int. Ed.* **2016**, *55*, 14310; *Angew. Chem.* **2016**, *128*, 14522; e) H.-Q. Xu, J. Hu, D. Wang, Z. Li, Q. Zhang, Y. Luo, S.-H. Yu, H.-L. Jiang, *J. Am. Chem. Soc.* **2015**, *137*, 13440.

[6] a) C. Wang, K. E. deKrafft, W. Lin, *J. Am. Chem. Soc.* **2012**, *134*, 7211; b) M. Wen, K. Mori, T. Kamegawa, H. Yamashita, *Chem. Commun.* **2014**, *50*, 11645; c) A. Fateeva, P. A. Chater, C. P. Ireland, A. A. Tahir, Y. Z. Khimyak, P. V. Wiper, J. R. Darwent, M. J. Rosseinsky, *Angew. Chem. Int. Ed.* **2012**, *51*, 7440; *Angew. Chem.* **2012**, *124*, 7558; d) Y. Horiuchi, T. Toyao, M. Saito, K. Mochizuki, M. Iwata, H. Higashimura, M. Anpo, M. Matsuoka, *J. Phys. Chem. C* **2012**, *116*, 20848; e) J.-D. Xiao, Q. Shang, Y. Xiong, Q. Zhang, Y. Luo, S.-H. Yu, H.-L. Jiang, *Angew. Chem. Int. Ed.* **2016**, *55*, 9389; *Angew. Chem.* **2016**, *128*, 9535; f) J. He, J. Wang, Y. Chen, J. Zhang, D. Duan, Y. Wang, Z. Yan, *Chem. Commun.* **2014**, *50*, 7063; g) L. Shen, M. Luo, L. Huang, P. Feng, L. Wu, *Inorg. Chem.* **2015**, *54*, 1191; h) D. Sun, W. Liu, Y. Fu, Z. Fang, F. Sun, X. Fu, Y. Zhang, Z. Li, *Chem. Eur. J.* **2014**, *20*, 4780; i) A. Dhakshinamoorthy, A. M. Asiri, H. Garcia, *ACS Catal.* **2017**, *7*, 2896.

[7] a) S. Linic, P. Christopher, D. B. Ingram, *Nat. Mater.* **2011**, *10*, 911; b) C. Wang, D. Astruc, *Chem. Soc. Rev.* **2014**, *43*, 7188; c) M. W. Knight, H. Sobhani, P. Nordlander, N. J. Halas, *Science* **2011**, *332*, 702; d) M. Bernardi, J. Mustafa, J. B. Neaton, S. G. Louie, *Nat. Commun.* **2015**, *6*, 7044; e) P. Zhang, T. Wang, J. Gong, *Adv. Mater.* **2015**, *27*, 5328.

[8] a) L. M. Liz-Marzán, C. J. Murphy, J. Wang, *Chem. Soc. Rev.* **2014**, *43*, 3820; b) K. Qian, B. C. Sweeny, A. C. Johnston-Peck, W. Niu, J. O. Graham, J. S. DuChene, J. Qiu, Y.-C. Wang, M. H. Engelhard, D. Su, E. A. Stach, W. D. Wei, *J. Am. Chem. Soc.* **2014**, *136*, 9842; c) Z. Bian, T. Tachikawa, P. Zhang, M. Fujitsuka, T. Majima, *J. Am. Chem. Soc.* **2014**, *136*, 458; d) B. Wu, D. Liu, S. Mubeen, T. T. Chuong, M. Moskovits, G. D. Stucky, *J. Am. Chem. Soc.* **2016**, *138*, 1114.

[9] a) M. Dan-Hardi, C. Serre, T. Frot, L. Rozes, G. Maurin, C. Sanchez, G. Férey, *J. Am. Chem. Soc.* **2009**, *131*, 10857; b) C. H. Hendon, D. Tiana, M. Fontecave, C. Sanchez, L. D′arras, C. Sassoye, L. Rozes, C. Mellot-Draznieks, A. Walsh, *J. Am. Chem. Soc.* **2013**, *135*, 10942; c) Z. Wang, X. Li, H. Xu, Y. Yang, Y. Cui, H. Pan, Z. Wang, B. Chen, G. Qian, *J. Mater. Chem. A* **2014**, *2*, 12571.

[10] X. Ye, L. Jin, H. Caglayan, J. Chen, G. Xing, C. Zheng, V. Doan-Nguyen, Y. Kang, N. Engheta, C. R. Kagan, C. B. Murray, *ACS Nano* **2012**, *6*, 2804.

[11] S. Sarina, H.-Y. Zhu, Q. Xiao, E. Jaatinen, J. Jia, Y. Huang, Z. Zheng, H. Wu, *Angew. Chem. Int. Ed.* **2014**, *53*, 2935; *Angew. Chem.* **2014**, *126*, 2979.

[12] A. Walsh, C. R. A. Catlow, *ChemPhysChem* **2010**, *11*, 2341.

[13] X. Pan, M. Yang, X. Fu, N. Zhang, Y.-J. Xu, *Nanoscale* **2013**, *5*, 3601.

[14] J.-X. Jian, Q. Liu, Z.-J. Li, F. Wang, X.-B. Li, C.-B. Li, B. Liu, Q.-Y. Meng, B. Chen, K. Feng, C.-H. Tung, L.-Z. Wu, *Nat. Commun.* **2013**, *4*, 2695.

Manuscript received: November 15, 2017
Accepted manuscript online: December 7, 2017
Version of record online: December 21, 2017

